*Sedimentology* (2009) **56,** 609–621 doi: 10.1111/j.1365-3091.2008.00988.x

# Large-scale intertidal polygonal features of the Abu Dhabi coastline

STEPHEN LOKIER and THOMAS STEUBER
*The Petroleum Institute, P.O. Box 2533, Abu Dhabi, United Arab Emirates (E-mail: slokier@pi.ac.ae)*

**ABSTRACT**

This study provides the first quantitative description of modern giant polygons. These large-scale, up to 166 m diameter, sedimentological features are described here in detail from the intertidal zone of the Arabian Gulf near Abu Dhabi. These features form by the displacive carbonate cementation of carbonate sand below a 3 to 5 cm thick cover of unconsolidated sediment. The oxygen isotopic composition of cements is consistent with precipitation from evaporated sea water. Cementation proceeds via a poorly consolidated layer that grades downward into an 8 to 14 cm thick, well-cemented grainstone. The margins of this expanding hardground form the overlapping borders of the polygons. Tepee structures at the borders of polygons are only occasionally preserved, as supporting sediment is removed by strong tidal currents and high-energy events, such as storms, that erode the unsupported tepees. These observations have clear implications for the use of tepees in the interpretation of ancient polygons and their associated environments. When preserved in the sedimentary record, tepee structures are interpreted to indicate lower energy depositional environments than that observed in this study.

**Keywords** Arabian Gulf, carbonate hardground, intertidal, polygon, tepee structures, UAE.

## INTRODUCTION

The southern shore of the Arabian Gulf comprises an extremely low-angle ramp setting characterized by supratidal evaporite precipitation passing offshore through a laterally extensive intertidal setting into subtidal carbonate deposition (Evans *et al.*, 1964; Alsharhan & Kendall, 2003). The shoreline is partially isolated from the more open marine conditions of the Arabian Gulf by a number of peninsulas and offshore islands (Fig. 1).

This study provides the first quantitative description of the distribution and morphology of very large-scale peritidal polygons that were identified over an extensive area during ongoing research into the sedimentological, depositional and diagenetic setting of the Abu Dhabi coastline. Large-scale polygons up to 166 m wide were identified from satellite images as occurring in the intertidal zone over an area measuring approximately 6·5 km long by 1·2 km wide. Kendall & Skipwith (1969) identified similar-scale polygons on intertidal sand flats 12 km to the west of the present study area. The Kendall and Skipwith study briefly described polygons that apparently bear distinct morphological differences from those described here.

Polygons have previously been described as ubiquitous features of the Abu Dhabi sabkha (Kendall & Skipwith, 1968; Kendall & Warren, 1987; Whittle *et al.*, 1998; Alsharhan & Kendall, 2003) and, indeed, of a number of other Recent depositional environments including the subtidal Arabian Gulf (Shinn, 1969), the intertidal flats and coastal salinas of Australia (Ferguson *et al.*, 1982; Warren, 1982) and the Great Basin playas of North America (Neal *et al.*, 1968; Warren, 2006). Polygons have also been widely described from the stratigraphic record, with examples from the Palaeozoic (Assereto & Kendall, 1977; Warren, 1983), Mesozoic (Assereto & Kendall, 1971; Smith, 1974; Bellamy, 1977; Tucker, 1981) and Cenozoic (Lugli *et al.*, 1999) being common.

Many of the previous studies of polygons, at all scales, have concentrated on the tepee structures

 

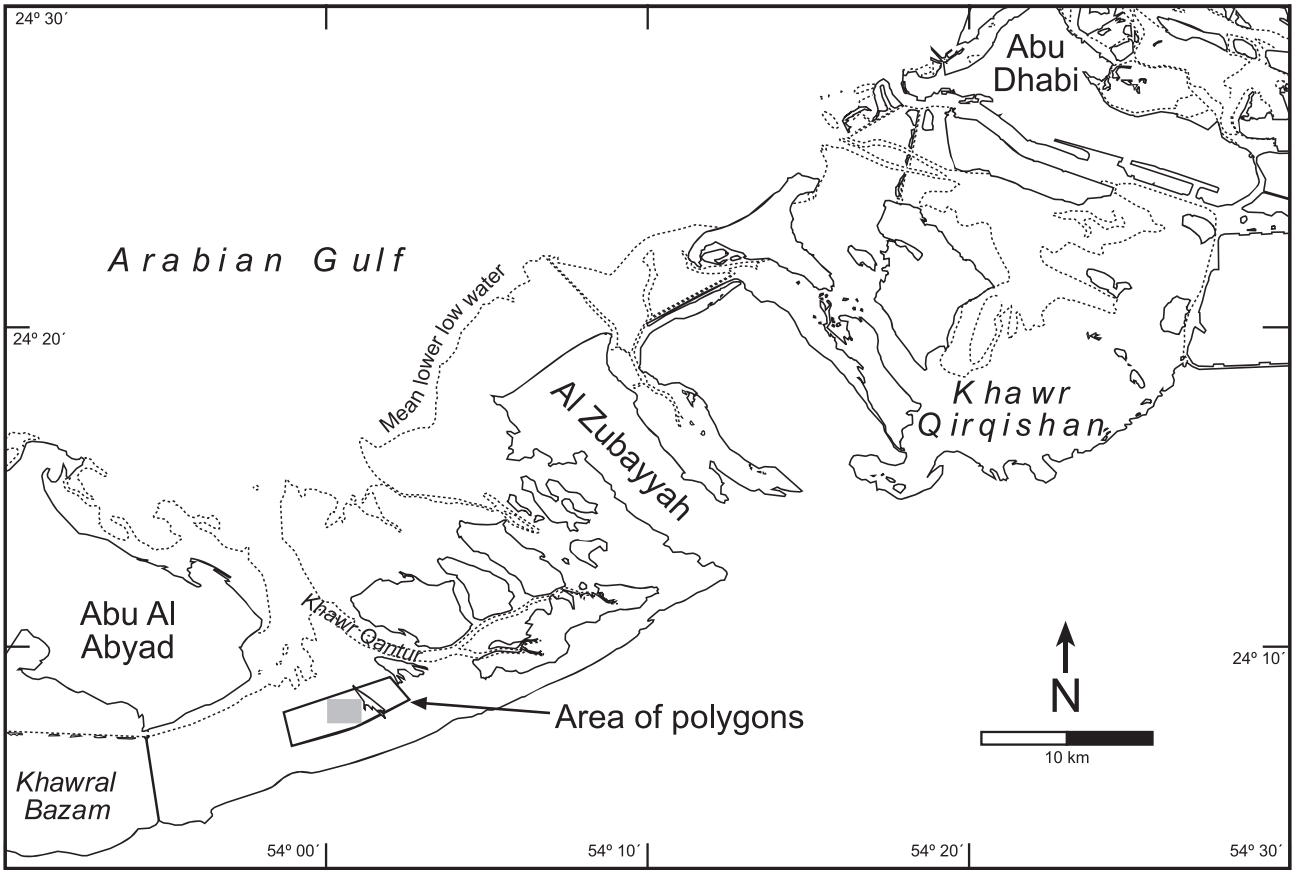


**Fig. 1.** Map of the UAE coastline between Abu Dhabi and Abu Al Abyad showing the location of the study area (shaded box). Note that the coastline is defined as mean higher high water. Mean lower low water is indicated by the dashed line.

that locally form at the polygon margins and have largely neglected the rest of the polygon system. This imbalance is addressed here by providing a quantitative description of all the morphological characteristics of the polygons. Petrographic and geochemical data are evaluated to offer an explanation of the mode of formation of the hardground and the polygons.

The new data and interpretations presented here have implications for the recognition and interpretation of ancient large-scale polygons within outcrop and core. In particular, the use of tepee structures as the primary diagnostic feature in the recognition of polygons and their associated environments is called into question.

## DESCRIPTION OF STUDY AREA

The study area is situated on the southern shore of the Arabian Gulf approximately 50 km to the south-west of Abu Dhabi city (Fig. 1). Initial satellite interpretation and field reconnaissance established an area of particularly well-developed polygons to the south-east of Abu Al Abyad Island as being ideal for detailed field-based observations (Figs 1 and 2).

The studied polygons are situated to the south of the Khawr Qantur channel within the intertidal zone of the north-west to south-east trending coastal complex (24°07·757′N, 054°01·301′E). The maximum spring tide range is 2 m. The area is characterized by hardgrounds with a thin (< 5 cm) cover of clean carbonate sands dominated by gastropods and peneroplid foraminifera skeletal material. To the south, the study area is bordered by microbial mats that pass landwards into the Abu Dhabi sabkha system. The eastern margin of the study area is a north-west to south-east aligned island with well-developed spits along the western coast; this island is joined to the mainland by a low causeway.

The arid climate of the UAE records a mean annual rainfall of 119 mm (United Arab Emirates University, 1993), with the majority (60%) of

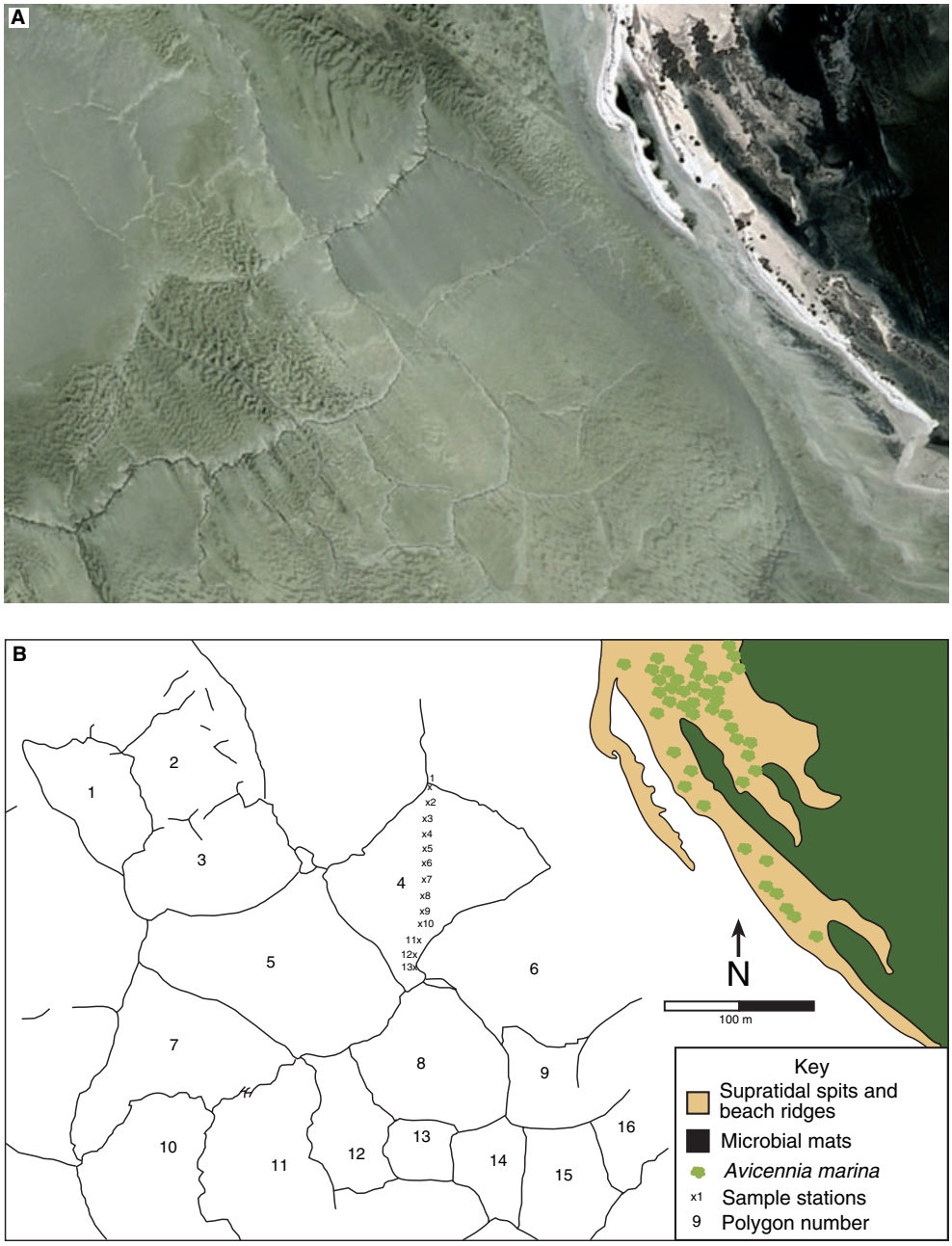


**Fig. 2.** QuickBird satellite image (A) of the study area and interpreted polygon distribution (B).

precipitation occurring during February and March as short-lived torrential events. Rainfall is highly variable on an annual basis, for example 282 mm was recorded during the winter of 1981 to 1982, while only 24 mm was recorded in 1984 to 1985. Annual temperature ranges between 8 °C in winter and 47 °C in summer were recorded between 2002 and 2007. Winds are dominated by the north-westerly Shamal which is particularly active during midwinter and summer days when gale-force winds can produce storm surges. The warm shallow water of the Arabian Gulf results in high humidity, particularly during the summer months when humidity can reach 100%.

Unreliable mapping and inconsistencies in transliteration have resulted in some confusion in the naming of geographical features in the Arabian Gulf region. In an attempt to alleviate this problem, the names of all geographical locations in this study have been derived from the admiralty charts as published by the UK Hydrographic Office (UKHO, 1997). These charts have been chosen as they follow a consistent format and are available widely.

## METHODOLOGY

The distribution and geometries of polygons were initially established using QuickBird satellite imagery (Fig. 2) and were subsequently ground-truthed during fieldwork. Boundaries between seven polygons were walked and examined in detail, with the characteristics of 458 m of boundary section being measured and described in terms of overall morphology, relief, orientation and dip direction. One polygon (Polygon 4 in Fig. 2) was selected for further detailed analysis, with a transect of 13 sampling stations being established at 10 m intervals across its surface. At each station, the thickness of the unconsolidated surface sediment was measured and a sample collected. A vertical 2·5 cm diameter plug was then drilled through the polygon and the thickness of poorly lithified and strongly lithified horizons recorded. The relief of the polygon at each station along the transect and at the polygon margins was measured accurately using ponded water within the polygon as a datum. Regular field visits over a period of two years allowed observations of annual changes in environmental conditions within the study area.

A total of 18 thin sections were prepared from the 13 plugs taken across Polygon 4. These thin sections were examined using standard light microscopy on a polarizing microscope to establish microfacies and cement phases. Rock chips from seven of the plugs were examined using scanning electron microscopy (SEM) to further characterize cements.

Radiocarbon analysis was undertaken via accelerator mass spectrometry (AMS) at the $^{14}$Chrono Centre, Queens University, Belfast. Results are presented as a conventional radiocarbon age using the Libby half-life method (Stuiver & Polach, 1977) and samples have been calibrated using the CALIB (version 5·0·1) calibration program (Stuiver & Reimer, 1993), utilizing a marine calibration curve and a regional reservoir age correction ($\Delta R$) of 180 ± 53 (Hughen *et al.*, 2004).

Water samples were collected throughout the study area and, for comparison, from more open-marine beaches on Abu Dhabi Island and at Jebel Dhanna, 150 km to the west of the study area. The oxygen isotopic composition of sea water samples was measured on carbon dioxide that was equilibrated with the water samples for 48 hours. External reproducibility, as defined by the standard deviation of multiple analysis of a laboratory standard, was better than 0·06‰ $\delta^{18}$O. Carbonate samples for the analysis of $\delta^{18}$O and $\delta^{13}$C were obtained with a tungsten drill bit (0·6 mm diameter) from plugs drilled through the hardground. External reproducibility is better than 0·1‰ $\delta^{18}$O and $\delta^{13}$C.

## DESCRIPTION OF POLYGONS

### Morphology

Polygons in the study area range in size up to 166 m across and typically belong to the irregular random orthogonal system as defined by Lachenbruch (1962). All the polygons studied exhibit a concave upward dish-like profile (Fig. 3), with margins having a relief of up to 17·7 cm above polygon centres. It is perhaps surprising that such large-scale features have not previously been described in detail; however, their sheer size coupled with their location in the lower intertidal zone makes identification at ground level difficult except during very low tides (Fig. 4).

Three types of polygon contact were identified during the study, which can be summarized as: (i) overlap borders; (ii) tepee borders; and (iii) gap borders (Fig. 5). Overlap borders account for 447·8 m (97·9%) of the total 458 m of the examined polygon contacts. These borders occur where the margin of a polygon overrides that of its neighbour with a resultant dip inclined towards the overriding polygon. Measured dip angles range between 1° and 32°, with the majority (57·7% of 52 measurements) having angles less than 6°. Overlap borders may occur either as simple single overlaps (57·3% of the length of the polygon borders) or as more complex multiple stacked overlaps (43·7% of examined border length).

Tepee borders are defined as contacts where polygon margins are in contact, uplifted and dip inwards towards their respective polygons to produce an 'inverted v-shape' profile as defined by Adams & Frenzel (1950) (Fig. 5C). The area below the tepee may be an empty void or may be filled by sediment. During the present study, only 6·3 m (1·4%) of the measured polygon borders exhibited tepee structures, and these had apex heights of 5 to 13 cm and widths of 13 to 60 cm, with dips ranging between 2° and 28° with a median of 6°.

Gap borders are the least common of the three classes of polygon contacts, accounting for only 3·5 m (0·8%) of measured borders. Gap borders are defined here as borders where margins between adjacent polygons have no physical contact (Fig. 5D). In all cases, the polygon

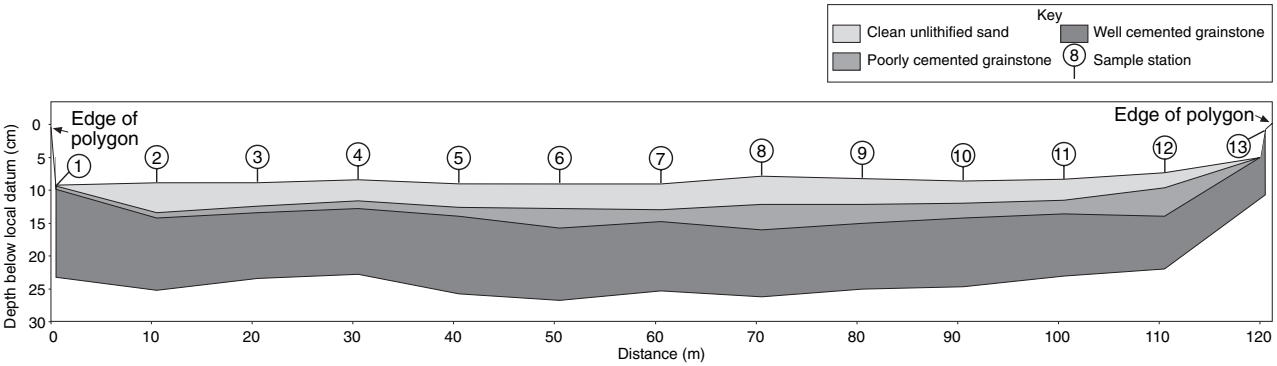


**Fig. 3.** Thickness of the clean unlithified sand, poorly lithified grainstone and well-lithified grainstone at each of the 13 sample stations. See Fig. 2 for the location of the sample stations.

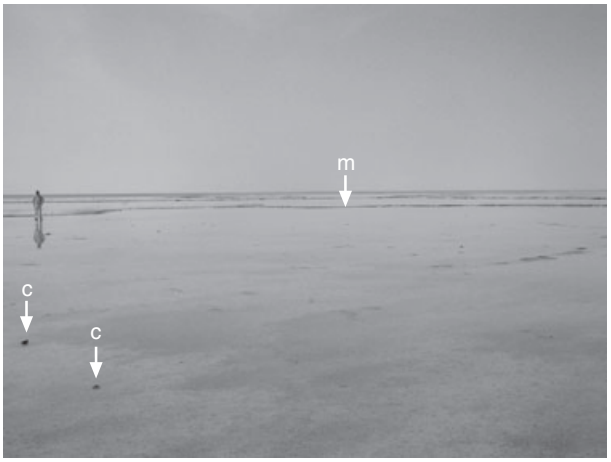


**Fig. 4.** Study area at low tide showing the extremely flat nature of the intertidal zone and the low relief of the polygon margins (m). Note the large cemented grainstone clasts (c) lying on the surface in the lower left corner of the image. Note figure for scale, 185 cm tall.

margins at gap borders were found to dip inwards towards their respective polygons with angles between 1° and 5°.

Uplifted borders typically exhibit evidence of dissolution with the strongest dissolution observed in the most uplifted examples. Encrusting bivalves and barnacles occur in the shaded areas on the underside of these borders. No intraclast breccias, as previously described from salina-formed (Warren, 1983) and subaqueous (Shinn, 1969) tepees, were observed at the polygon margins.

## Vertical profile

Unconsolidated surface sands overlie a poorly consolidated vuggy grainstone that passes down-section into a well-lithified grainstone (Fig. 3). Bioturbated, unconsolidated surface sediments show little variation in thickness (3·2 to 4·6 cm) over most of the polygon surface, with only the most steeply uplifted margins being clear of sediment. The unconsolidated surface sediment is dominated by rounded, fine upper to coarse lower sand-grade carbonate grains, the majority of which are derived from benthic foraminifera and gastropods. Angular, fine upper sand-grade detrital quartz is a minor component of the surface sediment. No mud-grade component is observed. The unconsolidated bioclastic sand exhibits a down-section change in colour from cream-brown at the sediment surface to grey at the contact with the underlying poorly consolidated grainstone. A distinct odour of $H_2S$ indicates active sulphate reduction. The underlying poorly consolidated horizon varies in thickness between 0·8 to 4·4 cm, with the greatest thicknesses observed closer to the polygon centres. The basal well-cemented grainstone shows little lateral thickness variation with a range of 8·0 to 13·3 cm. The lower boundary of the well-cemented layer is sharp and irregular, so that the cemented hardground lies on uncemented sediment. Loose clasts of well-cemented grainstone are scattered across the surface of the polygons (Fig. 4) and have been observed to have moved following storms. These boulder-sized clasts typically are tabular in nature and have thicknesses akin to those measured at polygon margins.

This study focuses on the morpholological rather than the petrographic characteristics of the polygons; therefore, thin-section and SEM analyses were only undertaken to establish the existence of any lateral or vertical variations in sediment composition or cement phases. The skeletal component of the bioclastic and peloidal grainstones is dominated by cerithid gastropods

 

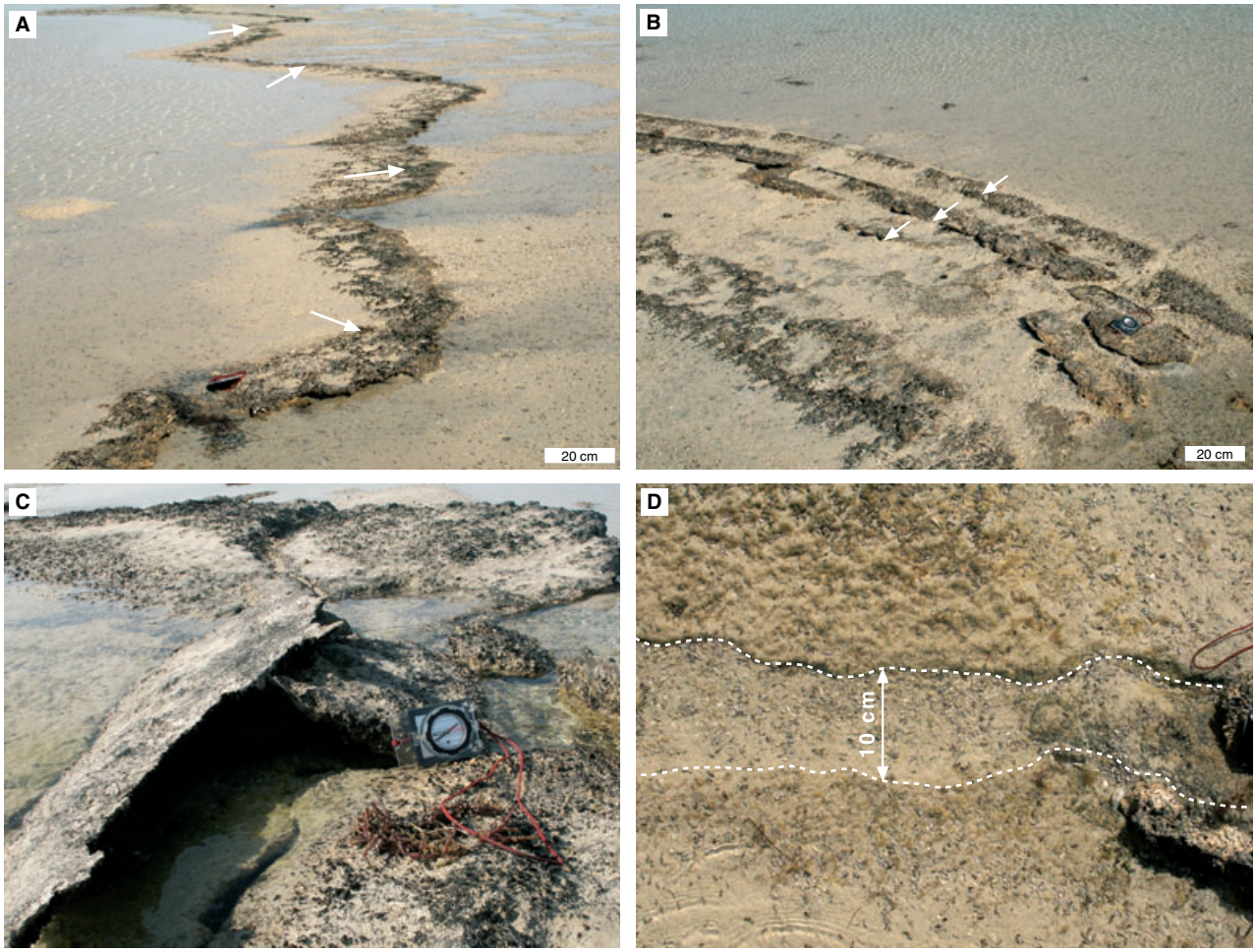


**Fig. 5.** The three main types of polygon border identified in the study. (A) Overlap border, arrows indicate the direction of overthrusting. (B) Area of multiple stacked overlaps, arrows indicate the direction of overthrusting. (C) Tepee border with an empty void below. (D) Gap border, note the cerithid gastropod-rich nature of the infilling sediment. Note that the compass–clinometer is 10 cm in length, the scale bars in images A and B represent horizontal distances in the image foreground.

and benthic foraminifera – particularly peneroplids and other miliolids. Other common bioclasts include bivalves and ostracods (Fig. 6). Many of the skeletal allochems are fragmented and have a micritized surface. Detrital angular quartz forms a minor component of the samples (Fig. 6). There is thus no difference between the major components of the cemented and unconsolidated sediments. Grain-rimming, typically isopachous, micrite cement is the primary cement within the lithologies. Many of the bioclasts contain an isopachous fringe of acicular aragonite; locally, a thin isopachous crust of prismatic high-Mg calcite coats the surface of bioclasts and peloids. Interparticle and intraparticle pores are common (Fig. 7). No lateral or vertical trends in facies or cement distribution were identified in the single polygon studied in detail.

## Salinity and isotope geochemistry

Measured salinities for water samples from the open-marine beaches at Abu Dhabi and Jebel Dhanna were significantly lower, 45 and 46 g $l^{-1}$, respectively, than those recorded from samples collected from the more restricted beaches within the study area, up to 75 g $l^{-1}$ (Table 1). The highest salinities, up to 89 g $l^{-1}$, were recorded from water samples ponding within polygons during low tides.

The $\delta^{18}O$ values of sea water are covariant with salinity ($n$ = 11, $r^2$ = 0·79) and range from 2·57‰ in samples from Abu Dhabi to 6·69‰ in waters ponding on polygons during low tide (Table 1). The oxygen and carbon isotopic compositions of four samples of aragonite cements (acicular and micritic) and a single gastropod range between

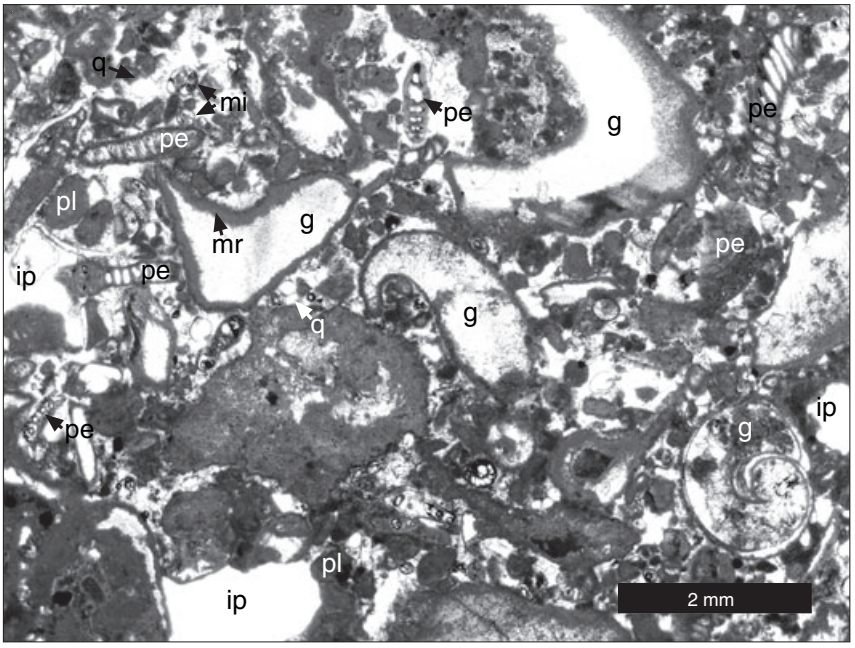


**Fig. 6.** Thin-section photomicrograph of the cemented grainstone horizon from Plug 2 of Polygon 4 (see Fig. 2B). The lithofacies is dominated by skeletal allochems and pelloids (pl). Many of the gastropods (g) are fragmented and exhibit micritized rims (mr). The foraminiferal assemblage is dominated by peneroplids (pe) along with other miliolids (mi). Intergranular porosity (ip) is common. Detrital quartz (q) is also observed.

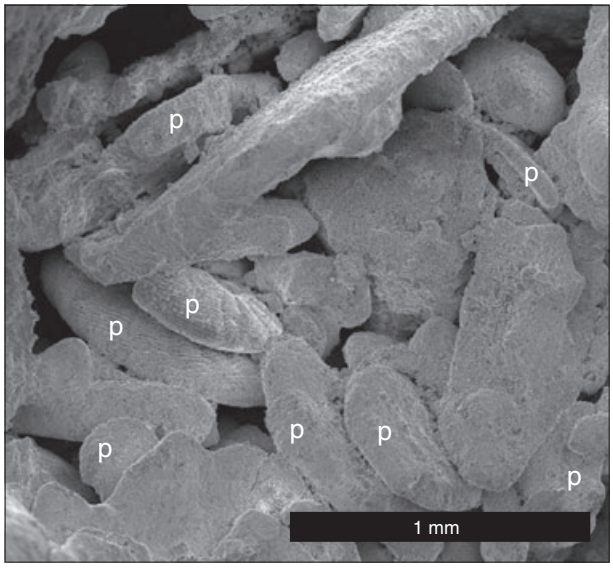


**Fig. 7.** SEM photomicrograph showing the high intergranular porosity within the cemented grainstone horizon. Note the high abundance of peneroplid foraminifera (p) within this sample (Plug 13 from Polygon 4).

3·29‰ and 4·20‰ $\delta^{18}$O, and between 1·31‰ and 1·71‰ $\delta^{13}$C, respectively (Table 2).

### Age

A radiocarbon age of 697 ± 26 BP was obtained from a single cerithid gastropod cemented at the upper surface of the poorly consolidated horizon at sample Station 6. This observation gives a calibrated age range ($2\sigma$) of 0 to 256 cal yr BP and is, therefore, taken as being equivalent to Recent.

## DISCUSSION

### Terminology

Despite widespread usage of the terms 'mega-polygon' and 'giant polygon', no formal definition has been identified and usage is inconsistent, with the terms variously being applied to describe features from as small as 1 m up to as large as 400 m in diameter (Table 3). Such a lack of consistency diminishes the value of these terms from a descriptive point of view. It is, therefore, proposed that the use of these terms be abandoned and that polygons are described in terms of their maximum and minimum dimensions.

### Mechanism of polygon development and evolution

Previous studies have proposed numerous mechanisms for the formation of peritidal and subaqueous polygons. Shinn (1969) suggested that the force of crystallization in subaqueous cemen-

 

**Table 1.** Temperature, salinity and $\delta^{18}O$ of seawater collected in the intertidal zone of the study region, and at Abu Dhabi and Jebel Dhanna beaches, the latter two locations representing more open-marine conditions than the study region.

| Sample description | Date | $T$ (°C) | Salinity (g $l^{-1}$) | $\delta^{18}O$ water (‰ V-SMOW) | $\delta^{18}O$ model aragonite (‰ V-PDB) |
|---|---|---|---|---|---|
| Study area, E shore, high tide, rising | 24/05/06 | 35·6 | 75 | 5·71 | 2·05 |
| Study area, W shore, high tide, rising | 24/05/06 | 35·1 | 61 | 5·07 | 1·52 |
| Abu Dhabi public beach | 25/05/06 | 30·5 | 45 | 2·57 | 0·08 |
| Study area, W shore, low tide, rising | 30/05/06 | 34·8 | 52 | 4·38 | 0·90 |
| Study area, E shore, high tide, falling | 31/05/06 | 34·2 | 54 | 4·16 | 0·83 |
| Study area, W shore, high tide, falling | 31/05/06 | 33·0 | 54 | 4·30 | 1·24 |
| Study area, W shore, tide falling | 29/11/06 | 27·3 | 61 | 3·89 | 2·14 |
| Jebel Dhanna north beach, high tide | 25/11/06 | 25·6 | 46 | 3·15 | 1·80 |
| Polygon, low tide | 21/08/06 | 39·7 | 75 | 5·14 | 0·54 |
| Polygon, low tide | 01/09/06 | 42·4 | 89 | 6·69 | 1·47 |
| Polygon, low tide | 11/10/06 | 35·3 | 89 | 5·39 | 1·81 |

The $\delta^{18}O$ values of model aragonite were calculated using the tabulated temperature and $\delta^{18}O_{water}$ data, following Goodwin *et al.* (2003).

**Table 2.** Oxygen and carbon isotopic values for aragonite cements and a single gastropod from the studied hardground.

| Sample number | Sample type | $\delta^{18}O$ (‰ V-PDB) | $\delta^{13}C$ (‰ V-PDB) |
|---|---|---|---|
| B153 | Carbonate cement | 1·31 | 3·99 |
| B155 | Carbonate cement | 1·71 | 3·42 |
| B158 | Carbonate cement | 1·48 | 4·20 |
| B159 | Carbonate cement | 1·49 | 4·01 |
| B156 | Gastropod | 1·62 | 3·29 |

ted hardgrounds resulted in the development of polygons observed on the sea floor of the Arabian Gulf. Kendall & Skipwith (1969) hypothesized that large-scale polygons south of Abu Al Abyad were formed either due to desiccation following subaerial exposure or from the accumulation of gases below a hardground. Kendall & Warren (1987) and Alsharhan & Kendall (2003) proposed formation of peritidal polygons via repeated diurnal contraction and expansion, with loose sediment entering cracks produced during contraction and 'wedging' the polygon open during the ensuing expansion phase. Assereto & Kendall (1977), however, suggested an initial phase of fracturing because of desiccation and thermal contraction during subaerial exposure, followed by marine vadose diagenesis during which lateral growth resulted from the force of crystallization combined with moisture swelling and thermal expansion.

Considering published figures for the thermal expansion of aragonite (Fei, 1995), a temperature change of 30 °C would result in a volume change of only 0·00025%. Therefore, the amount of diurnal, and even annual, expansion and contraction of the cemented polygons would be negligible with all movement being absorbed internally within the polygon slab. Thermal expansion and contraction processes therefore are ruled out as a viable mechanism for the lateral displacement required for polygon formation. The expansivity of carbonate rocks is also controlled by the moisture content of the rock (Hudec & Sitar, 1975). However, as all the studied hardgrounds are in a continuous state of saturation or near-saturation, it is inferred that isothermal expansion, caused by moisture content, can be rejected as an agent of polygon formation.

Desiccation fracturing is unlikely to be an effective process in the low cohesion, mud-free sediments from which the polygons described here are formed. Furthermore, no evidence of prolonged subaerial exposure was observed during two years of observation, and only the uplifted polygon margins are exposed briefly during low tide. Polygon formation because of the accumulation of gas is unlikely as the porous nature of the cemented hardground precludes the accumulation of sufficient trapped gas below this horizon.

Using the measured temperatures and $\delta^{18}O$ values of sea water (Table 1), the $\delta^{18}O$ values of aragonite are calculated according to Goodwin *et al.* (2003): $\delta^{18}O_{aragonite} = [(T - 20{\cdot}6) - (4{\cdot}34 \times (\delta^{18}O_{water} - 0{\cdot}2))] - 4{\cdot}34$. The $\delta^{18}O$ values of aragonite cements, and of a single gastropod, analysed from the hardground (Table 2) are consistent with precipitation from high-salinity

**Table 3.** Examples of usage of the terms 'megapolygon' and 'giant polygon'.

| Size (m) | Term used | Proposed mode of formation | Medium | Location | Age | Reference |
|---|---|---|---|---|---|---|
| 1–10 | Megapolygons | Early desiccation, cement growth, thermal expansion | Dolomite | Dolomites, Italy | Triassic | Assereto & Kendall (1977) |
| 1·5 | Megapolygons | Early desiccation, cement growth, thermal expansion | Limestone | Val Seriana, Italy | Triassic | Assereto & Kendall (1977) |
| 1·5–2 | Megapolygons | Desiccation, expansion, crystallization | Dolomite | Alps, Italy | Triassic | Assereto & Kendall (1971) |
| 3 | Megapolygons | Diurnal expansion and contraction | Limestone | Abu Dhabi, UAE | Recent | Alsharhan & Kendall (2003) |
| Up to 5 | Giant polygons | Desiccation | Halite | Agrigento, Sicily | Neogene | Lugli *et al.* (1999) |
| 5–10 | Megapolygons | Tectonic deformation of buried dolomite | Dolomite | Dorset, UK | Jurassic | Bellamy (1977) |
| 5–12 | Megapolygons | Hydraulic fracturing or thermal expansion and contraction | Limestone | Fisherman's Bay, Australia | Recent | Ferguson *et al.* (1982) |
| Up to 8 | Megapolygons | Early desiccation, cement growth, thermal expansion | Limestone | Atlas Mountains, Morocco | Jurassic | Assereto & Kendall (1977) |
| Up to 10 | Megapolygons | Early desiccation, cement growth, thermal expansion | Dolomite | Guadalupe Mountains, USA | Permian | Assereto & Kendall (1977) |
| Up to 14 | Giant polygons | Thermal contraction | Halite | Cheshire, UK | Triassic | Tucker (1981) |
| 40 | Megapolygons | Force of crystallization within fractures | Carbonate | Subtidal, Arabian Gulf | Recent | Kendall & Warren (1987) |
| 15–300 | Giant polygons | Desiccation | Mud | Great Basin Playas, USA | Recent | Neal *et al.* (1968) |
| ~400 | Megapolygons | Subaerial cementation and desiccation or gas accumulation below layer | Limestone | Abu Dhabi, UAE | Recent | Kendall & Skipwith (1969) |

water ponding on the polygons at temperatures between 35 and 42 °C (Table 1). The $\delta^{13}C$ values of aragonite also are consistent with those that would be expected for marine precipitates.

A substantial contribution of carbonate ions by the oxidation of organic matter via bacterial sulphate reduction would probably result in lower $\delta^{13}C$ values than those measured in the aragonite cements. However, the absence of isotope data for the marine dissolved inorganic carbon in this high-salinity environment precludes any further evaluation of the importance of sulphate reduction for aragonite cementation of the hardground.

It is concluded that the lateral growth of large-scale polygons is a contemporary process that is influenced primarily by the development of displacive carbonate cements, akin to the process suggested for subaqueous polygons by Shinn (1969). During low tides, the evaporation of marine water, retained in the dish-shaped polygons, produces supersaturated solutions which rapidly cement carbonate sediments at the surface of the polygons. Bacterial sulphate reduction, as evidenced by the formation of $H_2S$ and the grey colour of the sediment, where it grades into the poorly lithified layer, may provide carbonate ions necessary for cementation. Further displacive cementation within the lithified sediment results in expansion of the polygon outward to produce areas of compression and uplift. The lithified nature of the relatively thin cemented horizon results in fracturing of the uplifted areas to produce tepee structures, which are susceptible to erosion during high-energy events. With the removal of one side of the tepee, the unsupported side collapses to produce an overlap border. Occasionally, the margins of both polygons are removed and a gap border is produced.

The lower intertidal zone of the southern shoreline of the Arabian Gulf is described traditionally as a low-energy environment protected from higher energy open-marine conditions by offshore islands and peninsulas (Kendall & Skipwith, 1969). However, observations during the present study reveal the intertidal zone of the Abu Dhabi coastline to be a highly dynamic environment influenced by daily tidal currents and episodic high-energy events, particularly associated with the Shamal. The high-energy nature of the environment is reflected in the mud-free, rounded, relatively well-sorted nature of the surface sediments and the numerous tabular, boulder-sized, lithified, grainstone clasts lying on the polygon surface. The latter are interpreted as being sourced from uplifted polygon margins during episodic high-energy events such as storms.

The dissolution observed on uplifted polygon borders is inferred to be produced through meteoric dissolution as water condenses onto exposed polygon borders during periods of elevated humidity. It is hypothesized that the very large size of the polygons described in this study may result from the relatively thick nature of the well-cemented hardground. With continued vertical cementation of the sediment pile and increasing thickness of the hardground, the margins of these early polygons would have been obliterated to leave only the large-scale polygons described here.

## Types of polygon borders and implications for the formation and preservation of tepee structures

As discussed earlier, tepee borders are interpreted to form via the uplift of the polygon surface during lateral expansion associated with displacive cement development (Figs 8 and 9). However, tepees are relatively rare as their uplifted nature makes them particularly susceptible to erosion during high-energy events. Overlap borders dominate the border types observed during this study, and are interpreted to result from the lateral displacement of a polygon margin over that of its neighbour following tepee collapse (Fig. 8). The distance to which a border can override will be limited by the mechanical strength of the pushed slab; where this fails, a new overriding border front will be initiated to result in multiple stacked overlap borders (Fig. 5B). Gap borders are interpreted as transient features of the polygon margin as they represent areas where a tepee or overlap border has been removed, yet polygon growth has not yet filled the space between the adjacent polygons (Fig. 9).

There is no previously published classification of intertidal polygon boundaries. The closest possible analogue to the system proposed here is that of Shinn (1969) for sub-tidal polygons; however, there are several important differences. True tepee structures are rare in the intertidal polygons but appear to be common in the subaqueous system. In the case of subaqueous polygons, fragments of hardground are described as recementing at the polygon border, and no such process is observed in the intertidal zone polygons described here. Intertidal polygon margins display irregular, solution-degraded upper

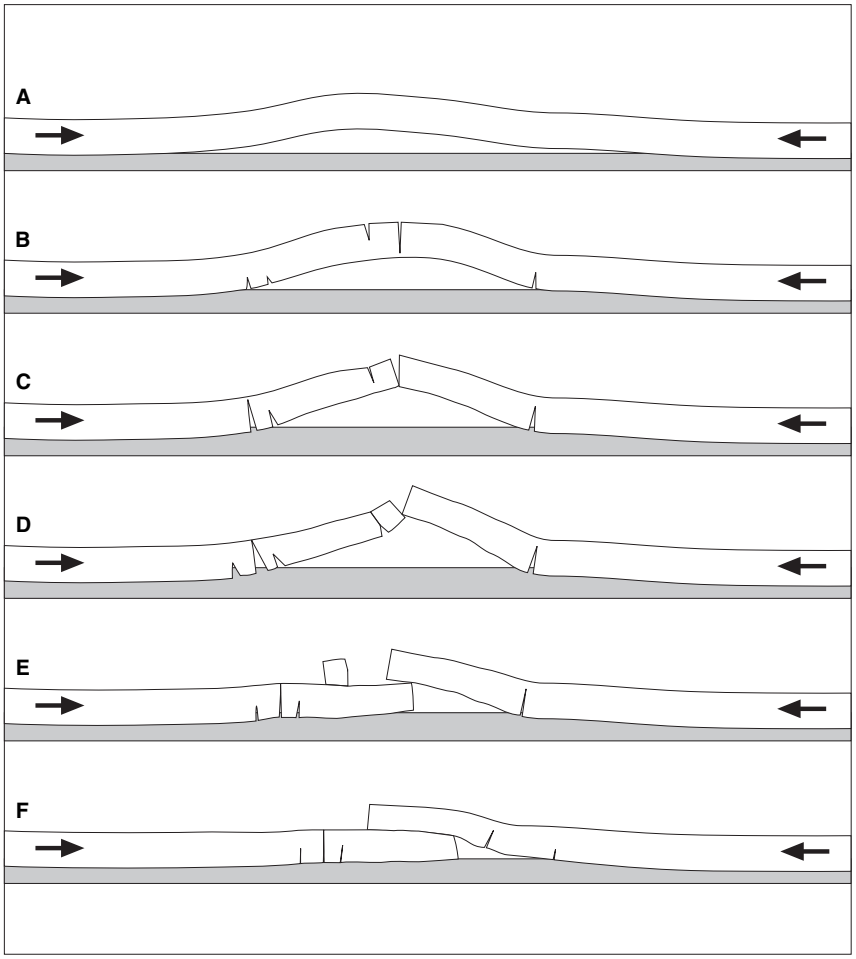


**Fig. 8.** Schematic of the development of an overlap border. The growth of displacive cements results in the outward growth of the cemented layer to produce zones of compression and uplift (A) with resultant fracturing (B). Continued lateral displacement forms a tepee structure (C) which will eventually become unstable (D) and susceptible to collapse (E); where only one side of the tepee is broken away, an overlap border will result. With the continued growth of displacive cements further expansion results in the thrusting of the overlying margin to form an overlap border (F).

surfaces that are quite distinct from the eroded and bored flattened surfaces described from subtidal polygon margins. The lineations described from the overthrust margins of subaqueous polygons are not observed in the intertidal polygons.

## Implications for the recognition of ancient intertidal polygons

Previous polygon studies have concentrated on the recognition of ancient tepee structures in outcrop and core to interpret a number of environments of polygon formation, including the intertidal zone. In low-energy environments, uplifted borders, including tepees, may act as sediment traps, with the sediment deposited below these structures supporting them and enhancing preservation. Yet, in the relatively high-energy intertidal zone of this study, a lack of sediment below uplifted borders makes tepees particularly vulnerable to collapse and erosion, with little chance of preservation (Figs 8 and 9). Borders form a limited portion of the surface area of the very large polygons examined during this study; tepees comprise only a minor percentage of these borders. Thus, tepees will be relatively rare features in outcrop and are extremely unlikely to be sampled in core. The occurrence of abundant tepees in outcrop or core therefore is inferred to indicate a low-energy environment of formation and is inconsistent with a high-energy setting such as that observed during this study.

Overlap borders will be much more common; in outcrops, these may be identified as a dislocated layer of strata with a dip inwards towards the centre of the host polygon (Fig. 8). The overriding border may exhibit some evidence of dissolution; the underside may be encrusted by marine biota.

 

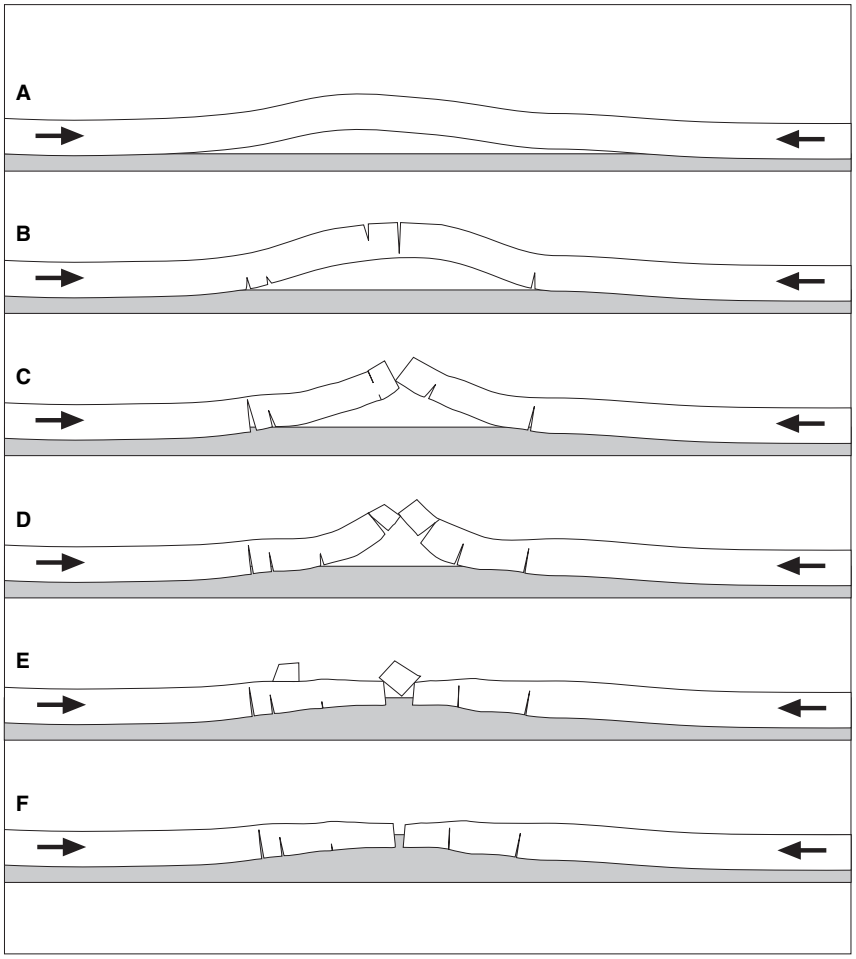


**Fig. 9.** Schematic of the development of a gap border. Displacive cement growth results in the lateral displacement of the cemented layer to produce zones of compression and uplift (A) and associated fracturing (B). Continued displacement forms a tepee border (C) which becomes unstable (D) and collapses (E); where both sides of the tepee are broken away, a gap border is formed. With the continued precipitation of displacive cements, further expansion closes the gap (F) and the process may be repeated.

In the core, overlap borders may be more difficult to recognize as they will simply appear as two successive layers of early-cemented lithology. Again, dissolution and the occurrence of encrusting biota on the underside of the upper horizon may aid recognition.

As gap borders are interpreted as transient features (Fig. 9), following the removal of tepee or overlap borders, it is hypothesized that their preservation would be rare. Where gap borders are preserved, they would be identified in outcrop as a lateral gap in a horizon; in cores, it would be very difficult to conclusively identify a gap border.

## CONCLUSIONS

Giant polygons are quantitatively described from the lower intertidal zone of the southern Arabian Gulf, *ca* 50 km to the West of Abu Dhabi. The polygons described here have diameters of up to 166 m and are formed by cementation from evaporated sea water of carbonate sands rich in benthic foraminifera and gastropods. Cementation occurs below a 3·2 to 4·6 cm thick cover of unconsolidated sediment of similar composition and is probably facilitated by bacterial sulphate reduction.

Formation of displacive carbonate cement is considered to cause an outward expansion of polygons, which results in uplift, fracturing and overthrusting of polygon borders. Three types of polygon borders are recognized. Overlap borders dominate by far (97·8% of border length), while tepee and gap borders are subordinate. Tepees are a transient feature in the relatively high-energy setting studied here, and are destroyed either by high-energy events, such as storms, or eventually collapse because of the lack of sediment accumu-

lation that may support them in lower energy settings. Therefore, the polygon boundaries described here may be difficult to recognize as such in ancient sedimentary rocks, particularly in core sections.

## ACKNOWLEDGMENTS

The authors would like to thank reviewer B. Charlotte Schreiber, an anonymous reviewer, and editor Peter Swart for their detailed comments and suggestions during the review process. Elaine Richardson kindly carried out proof-reading. We thank Alan Cocks for assistance in the field.

## REFERENCES

**Adams, J.E.** and **Frenzel, H.N.** (1950) Capitan barrier reef, Texas and New Mexico. *J. Geol.*, **58,** 289–312.

**Alsharhan, A.S.** and **Kendall, C.G.St.C.** (2003) Holocene coastal carbonates and evaporites of the southern Arabian Gulf and their ancient analogue. *Earth-Sci. Rev.*, **61,** 191–243.

**Assereto, A.L.** and **Kendall, C.G.St.C.** (1971) Megapolygons in Ladinian limestones of Triassic of Southern Alps: Evidence of deformation by penecontemporaneous desiccation and cementation. *J. Sed. Petrol.*, **41,** 715–723.

**Assereto, A.L.** and **Kendall, C.G.St.C.** (1977) Nature, origin and classification of peritidal tepee structures and related breccias. *Sedimentology*, **24,** 153–210.

**Bellamy, J.** (1977) Subsurface expansion megapolygons in Upper Jurassic dolostone (Kimmeridge, UK). *J. Sed. Res.*, **47,** 973–978.

**Evans, G., Kinsman, D.J.J.** and **Shearman, D.J.** (1964) A reconnaissance survey of the environment of recent carbonate sedimentation along the Trucial Coast, Persian Gulf. In: *Developments in Sedimentology*, vol. 1. *Deltaic and Shallow Marine Deposits: Proceedings of the 6th International Sedimentological Congress, The Netherlands and Belgium – 1963* (Ed. L.M.J.U. Van Straaten), pp. 129–135. Elsevier, Amsterdam.

**Fei, Y.** (1995) Thermal expansion. In: *Mineral Physics and Crystallography: A Handbook of Physical Constants AGU Reference Shelf 2* (Ed. T.J. Ahrens), pp. 29–44. American Geophysical Union, Washington, DC.

**Ferguson, J., Burne, R.V.** and **Chambers, L.A.** (1982) Lithification of peritidal carbonates by continental brines at Fisherman Bay, South Australia, to form a megapolygon/spelean limestone association. *J. Sed. Res.*, **52,** 1127–1147.

**Goodwin, D.H., Schöne, B.R.** and **Dettman, D.L.** (2003) Resolution and fidelity of oxygen isotopes as palaeotemperature proxies in bivalve mollusk shells: models and observations. *Palaios*, **18,** 110–125.

**Hudec, P.P.**. and **Sitar, N.** (1975) Effect of water sorption on carbonate rock expansivity. *Can. Geotech. J.*, **12,** 179–186.

**Hughen, K.A., Baillie, M.G.L., Bard, E., Bayliss, A., Beck, J.W., Blackwell, P.G., Buck, C.E., Burr, G.S., Cutler, K.B., Damon, P.E., Edwards, R.L., Fairbanks, R.G., Friedrich, M., Guilderson, T.P., Herring, C., Kromer, B., McCormac, F.G., Manning, S.W., Ramsey, C.B., Reimer, P.J., Reimer, R.W., Remmele, S., Southon, J.R., Stuiver, M., Talamo, S., Taylor, F.W., van der Plicht, J.** and **Weyhenmeyer, C.E.** (2004) Marine04 Marine radiocarbon age calibration, 0–26 cal kyr BP. *Radiocarbon*, **46,** 1059–1086.

**Kendall, C.G.St.C.** and **Skipwith, P.A.** (1968) Recent algal mats of a Persian Gulf lagoon. *J. Sed. Petrol.*, **38,** 1040–1058.

**Kendall, C.G.St.C.** and **Skipwith, P.A.** (1969) Geomorphology of a Recent shallow-water carbonate province: Khor Al Bazam, Trucial Coast, Southwest Persian Gulf. *Geol. Soc. Am. Bull.*, **80,** 865–891.

**Kendall, C.G.St.C.** and **Warren, J.** (1987) A review of the origin and setting of tepees and their associated fabrics. *Sedimentology*, **34,** 1007–1027.

**Lachenbruch, A.H.** (1962) Mechanics of thermal contraction cracks and ice wedge polygons in permafrost. Geol. Soc. Am. Spec. Paper, 70, 69 pp.

**Lugli, S., Schreiber, B.C.** and **Triberti, B.** (1999) Giant polygons in the Realmonte Mine (Agrigento, Sicily): evidence for the desiccation of a Messinian halite basin. *J. Sed. Res.*, **69,** 764–771.

**Neal, J.T., Langer, A.M.** and **Kerr, P.F.** (1968) Giant desiccation polygons of Great Basin playas. *Geol. Soc. Am. Bull.*, **79,** 69–90.

**Shinn, E.A.** (1969) Submarine lithification of Holocene carbonate sediments in the Persian Gulf. *Sedimentology*, **12,** 109–144.

**Smith, D.B.** (1974) Origin of tepees in Upper Permian shelf carbonate rocks of Guadalupe Mountains, New Mexico. *AAPG Bull.*, **58,** 63–70.

**Stuiver, M.** and **Polach, H.A.** (1977) Discussion: Reporting of $^{14}C$ data. *Radiocarbon*, **19,** 355–363.

**Stuiver, M.** and **Reimer, P.J.** (1993) Extended $^{14}C$ data base and revised CALIB 3.0 $^{14}C$ age calibration program. *Radiocarbon*, **35,** 215–230.

**Tucker, R.M.** (1981) Giant polygons in the Triassic salt of Cheshire, England: a thermal contraction model for their origin. *J. Sed. Petrol.*, **51,** 779–786.

**UKHO** (1997) *Outer Approaches to Abu Dhabi (Abu Zaby) (Chart 3177)*. United Kingdom Hydrographic Office. Taunton.

**United Arab Emirates University** (1993) *The National Atlas of The United Arab Emirates*. UAE University, Al Aln, UAE, 175 pp.

**Warren, J.K.** (1982) The hydrological significance of Holocene tepees, stromatolites, and boxwork limestones in coastal salinas in South Australia. *Sed. Geol.*, **34,** 1–19.

**Warren, J.K.** (1983) Tepees, modern (southern Australia) and ancient (Permian – Texas and New Mexico) – a comparison. *J. Sed. Petrol.*, **52,** 1171–1201.

**Warren, J.K.** (2006) *Evaporites: Sediments, Resources and Hydrocarbons*. Springer-Verlag, Berlin, 1036 pp.

**Whittle, G.L., Alsharhan, A.S.** and **Kendall, C.G.St.C.** (1998) Petrography of Holocene beachrock and hardgrounds, Abu Dhabi, United Arab Emirates. In: *Quaternary Deserts and Climate Change* (Eds A.S. Alsharhan, K.W. Glennie, G.I. Whittle and C.G.St.C. Kendall), pp. 57–68. A. A. Balkema, Rotterdam.

*Manuscript received 18 September 2007; revision accepted 21 May 2008*

 